Triblock SEBS/DVB crosslinked and sulfonated membranes: fuel cell performance and conductivity

R. Teruel-Juanes[1], C. del Río[2], O. Gil-Castell[1], C. Primaz[1], A. Ribes-Greus[1,*]

DOI:

https://doi.org/10.1002/app.50671

Please, cite it as:

Teruel-Juanes R, del Río C, Gil-Castell O, Primaz C, Ribes-Greus A. Triblock SEBS/DVB crosslinked and sulfonated membranes: Fuel cell performance and conductivity. Journal of Applied Polymer Science. 2021;e50671.

[1]Instituto de Tecnología de Materiales (ITM), Universitat Politècnica de València (UPV). Camino de Vera s/n, 46022 Valencia, Spain.

[2]Instituto de Ciencia y Tecnología de Polímeros (ICTP–CSIC), Juan de la Cierva 3, 28006 Madrid, Spain

[*]Corresponding author:

A. Ribes-Greus aribes@ter.upv.es

Triblock SEBS/DVB crosslinked and sulfonated membranes: fuel cell performance and conductivity

R. Teruel-Juanes[1], C. del Río[2], O. Gil-Castell[1], C. Primaz[1], A. Ribes-Greus[1,*]

[1]Instituto de Tecnología de Materiales (ITM), Universitat Politècnica de València (UPV). Camino de Vera s/n, 46022 Valencia, Spain.

[2]Instituto de Ciencia y Tecnología de Polímeros (ICTP–CSIC), Juan de la Cierva 3, 28006 Madrid, Spain

[*]Corresponding author:

A. Ribes-Greus aribes@ter.upv.es

Abstract

A set of styrene-ethylene-butylene-styrene triblock copolymer (SEBS) membranes with 10 or 25 wt.% divinyl-benzene (DVB) as a crosslinking agent were prepared and validated. Physicochemical characterization revealed suitable hydrolytic and thermal stability of photo-crosslinked membranes containing 25%wt. DVB and post-sulfonated. These compositions were evaluated in H_2/O_2 single cells, and electrical and proton conductivities were furtherly assessed. The membranes with the milder post-sulfonation showed greater proton conductivity than those with excessive sulfonation. In terms of electrical conductivity, a universal power law was applied, and the values obtained were low enough for being used as polyelectrolytes. At the analyzed temperatures, the charge transport process follows a long-range pathway or vehicular model. Finally, fuel cell performance revealed the best behavior for the membrane with 25 wt.% DVB, photo-crosslinked during 30 min and mild sulfonated, with a promising power density of 526 $mW \cdot cm^{-2}$. Overall, the results obtained highlight the promising fuel cell performance of these cost-effective triblock copolymer-based membranes and indicate that higher sulfonation does not necessarily imply better power density.

1. Introduction

The production of clean and sustainable energy is one of the greatest challenges of the twenty-first century. Currently, around 80% of the total energy demand comes from fossil fuels, resulting in pollutants and greenhouse gas emissions such as carbon dioxide. Therefore, alternative energy sources are being explored during the last decades and becoming essential. Among them, fuel cells (FC) are eco-friendly and high-efficiency devices for the electrochemical conversion of fuel chemical energy into electricity [1,2].

Among all, proton exchange membrane fuel cells (PEMFCs) have attracted much attention from the research community due to their high energy density and low operation temperature which permits a rapid start-up and wide application variety. PEMFC is the only low-temperature fuel cell type that uses a solid material as an electrolyte, namely a proton exchange membrane (PEM), whose unique features have overpowered the classical liquid electrolyte systems. Apart from the standard perflurosulfonic acid membranes (Nafion® type) whose benefits as well as severe drawbacks are widely known [3], the development of alternative PEMs is the driving force of numerous researchers to attain the expansion of this technology. Although the progress of new PEMs has maturated significantly during the last decade, there are still technological barriers to overcome, such as thermal and mechanical stability in wet states, fuel crossover, and competitive cost. Thereby, the development of more affordable PEMs based on hydrocarbon structures of sulfonated aromatic polymers may involve incentive and cost-effective opportunities in this field. Numerous examples of potential membrane materials functionalized with sulfonic groups have been proposed and can be found in the recent related bibliography such as poly(ether-ether ketones) [4–7], poly(vinyl alcohol) [8–12], polyimides [13–16], poly(benzimidazoles) [17–20], poly(phosphazenes) [21–23] or polystyrene-block copolymers [24–27].

In particular, PEMs based on polystyrene-containing block copolymers give rise to interesting possibilities as a result of their low cost, good processability, and easy functionalization capability. Styrene-ethylene-butylene-styrene (SEBS) is a commercially available terpolymer proposed for proton exchange membrane fabrication. SEBS is obtained by full hydrogenation of styrene-butadiene-styrene (SBS) thermoplastic elastomer to prevent undesirable side reactions in the non-aromatic double bonds during functionalization. It is well established that high degrees of functionalization in SEBS are needed to achieve adequate proton conductivity values [28]. Nevertheless, a linear relationship between both factors does not always imply a better behavior so a suitable balance between swelling, conducting properties, and dimensional

stability of the membrane has been demonstrated to be critical for avoiding an early degradation in humid environments and achieving a suitable cell performance. Previously, it was demonstrated that UV photo-crosslinking of SEBS-DVB membranes delivered the desired effects of reducing swelling in water and improving dimensional stability without altering the number of aromatic rings available for post-sulfonation reaction [29].

In this work, a series of photo-crosslinked and post-sulfonated SEBS-based membranes with divinyl-benzene (DVB) were prepared, evaluated, and optimized in terms of the crosslinking agent percentage, photo-crosslinking doses, and post-sulfonation conditions. Although the characterization in terms of hydrothermal stability, chemical structure, thermo-oxidative stability, and thermal properties may be useful to define the optimal composition of a membrane to be tested in H_2/O_2 single cells, a complementary evaluation of the control mechanisms of ion transport should provide extensive knowledge on the fuel cell performance. In this regard, a comprehensive analysis of electrical and protonic conductivity appears is crucial for a successful design and validation of advanced selective transport materials for proton exchange membranes. For this purpose, in this study broadband dielectric spectroscopy, a powerful tool for determining the electrical properties and their relation with macromolecular dynamics was used to evaluate the control mechanisms of ion transport. The two components of electrical conductivity, alternating current (AC) and the direct current (DC), were modeled by a universal power law and by the relationship between the real and imaginary impedance on the frequency from the Bode plots, respectively. Finally, the results obtained were correlated to the fuel cell performance, which contributed to one-step further on the development of triblock SEBS/DVB photo-crosslinked and sulfonated membranes.

2. Materials and methods

2.1. Materials

The main component of the membranes was styrene-ethylene-butylene-styrene (SEBS) triblock copolymer with 32 wt.% of styrene units, grade Calprene CH-6120 (Repsol). As the crosslinking agent, divinylbenzene (DVB) (Sigma-Aldrich) was used and 2,2-dimethoxy-1,2-diphenyletan-1-one, grade Irgacure 651 (Ciba) was considered as photo-initiator. The sulfonation agent was thrimethylsilyl chlorosulfonate 99% (Sigma-Aldrich) and other solvents used for membrane development were chloroform ($CHCl_3$) (Scharlau) and 1,2-dichlorethane (DCE) (Scharlau). A membrane of Nafion 117® was used as reference, which was pre-treated

by immersion in three consecutive baths of 3% H_2O_2, 0.5 M H_2SO_4, and distilled water, as described in the literature [30].

2.2. Membrane preparation: photo-crosslinking and post-sulfonation

SEBS and DVB were dissolved in chloroform with the following proportions: SEBS-DVB 90-10 wt.% and SEBS-DVB 75-25 wt.%. Both dissolutions included a 2% of 2,2-dimethoxy-1,2-diphenyletan-1-one as photo-initiator by weight percentage of DVB. Subsequently, the membranes were prepared using the doctor blade casting technique. After casting, the membranes were left in darkness, allowing for the chloroform evaporation during 2 h. Once dry, the obtained membranes were irradiated at room temperature using UV spotlight irradiation from Hamamatsu L8868 with a 200 W Hg-Xe non-filtrated lamp. The intensity of the incident light was focused on the samples with an optical fiber positioned at 8 cm from the treated membranes. The irradiation process was carried out for either 15 or 30 min. To remove the non-crosslinked DVB, the obtained membranes were washed with 1,2-dichlorethane (DCE). Subsequently, they were subjected to a heterogeneous sulfonation process through immersion in trimethylsilyl chlorosulfonate/DCE solutions with dissimilar conditions: 2 h immersion in 0.3 M or 3 h immersion in 0.5 M solution. Afterward, the obtained membranes were washed with deionized water until neutral pH was reached. Finally, a drying stage during 24 h at 50 °C was considered before storage. The experimental approach for the preparation of the membranes is summarized in **Figure 1** and the composition and designation of the obtained membranes according to the different preparation steps (blending, UV-irradiation and post-sulfonation) are shown in **Table 1**.

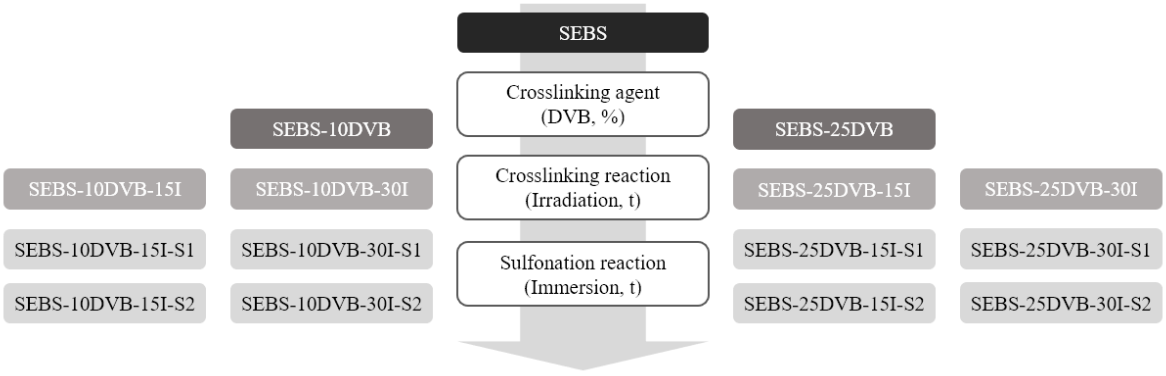

Figure 1. Experimental approach for the preparation of the membranes: blending, photo-crosslinking, and post-sulfonation.

Table 1. Composition and obtaining conditions along with the designation of the obtained SEBS-based membranes.

Composition		UV-irradiation time(min)	Post-sulfonation conditions	Designation
SEBS (wt.%)	DVB (wt.%)			
100	-	-	-	SEBS
90	10	-	-	SEBS-10DVB
		15	-	SEBS-10DVB-15I
			0.3 M for 2 h	SEBS-10DVB-15I-S1
			0.5 M for 3 h	SEBS-10DVB-15I-S2
		30	-	SEBS-10DVB-30I
			0.3 M for 2 h	SEBS-10DVB-30I-S1
			0.5 M for 3 h	SEBS-10DVB-30I-S2
75	25	-	-	SEBS-25DVB
		15	-	SEBS-25DVB-15I
			0.3 M for 2 h	SEBS-25DVB-15I-S1
			0.5 M for 3 h	SEBS-25DVB-15I-S2
		30	-	SEBS-25DVB-30I
			0.3 M for 2 h	SEBS-25DVB-30I-S1
			0.5 M for 3 h	SEBS-25DVB-30I-S2

2.3. Swelling and hydrothermal stability

The membranes were preliminarily validated employing swelling and hydrothermal stability analyses. For this purpose, the membranes were immersed in water at 60 °C and the mass was gravimetrically monitored as a function of time. In particular, 20 mL vials were filled with distilled water and introduced into a stove. Then, fully dried samples were introduced and sequentially extracted, dried, weighed, and introduced again into the vials. Different extractions were planned, one extraction each 15 min during 300 min and a final extraction after 500 min. The percentage of absorbed solvent was calculated as the mass difference between the immersed samples (M_t) and the dry sample (M_0), as shown in **Equation 1**. The mass variation at saturation (M_s) corresponds to the percentage when the equilibrium was reached [31].

$$M_s\ (\%) = \frac{M_t - M_0}{M_0} \times 100 \qquad (1)$$

2.4. Membrane characterization

2.4.1. Fourier Transform Infrared Spectroscopy (FT-IR)

The FTIR analysis was performed using a Thermo Nicolet 5700 FT-IR spectrometer. The infrared spectra of prepared membranes were collected in the attenuated total reflectance (ATR) mode in the wavenumber range between 500 to 4000 cm^{-1}, with 64 accumulations. Five analyses per sample were performed and averaged.

2.4.2. Differential scanning calorimetry (DSC)

The differential scanning calorimetry (DSC) analyses were evaluated using a Mettler Toledo DSC822^e equipment. Aluminum capsules were filled with the samples, with a mass between 2 and 4 mg, and sealed. Then, they were subjected to a heating/cooling program with a rate of 30 °C·min^{-1} in the temperature range from -20 °C to 200 °C under an inert atmosphere of nitrogen with a flow rate of 50 mL·min^{-1}.

2.4.3. Thermogravimetric analysis (TGA)

The thermogravimetric analysis (TGA) was carried out with a Mettler Toledo TGA/STDA 851^e setup. The samples, with a mass between 2 and 5 mg were placed into 70 µL alumina capsules. Analyses were performed with a heating rate of 30 °C·min^{-1} over the 30 °C to 800 °C temperature range. An empty capsule was used as a blank to take the reference baseline. The analyses were carried out using an oxidative atmosphere with a flux of 50 mL·min^{-1} of oxygen.

2.5. Membrane validation

2.5.1. Fuel cell performance

Membranes were sandwiched between electrodes to fabricate the membrane-electrodes assemblies (MEAs). The catalyst layers for both anode and cathode consisted of Pt/C (40% Pt on Vulcan XC-72, E-TEK) with a Pt load of 1.00 ± 0.07 mgPt·cm^{-2}. The active area of the MEA was 5 cm^2 and a commercial cell hardware ElectroChem Inc. was used for the electrochemical experiments. Performance tests of the MEAs were carried out using a Scribner 850e multi-range fuel cell test system using H_2 and O_2 (200 mL·min^{-1}) at atmospheric pressure. The tests were run at 60 °C and 70 °C and 100% relative humidity.

2.5.2. Dielectric thermal impedance spectroscopy (DETA)

The impedance measurements were conducted using a Novocontrol Broadband Dielectric Impedance Spectrometer, connected to a Novocontrol Alfa-A Frequency Response Analyzer. Frequency varied in the range from 10^{-2} to 10^{-7} Hz and temperature from 10 to 90 °C. All the measurements were obtained under isothermal conditions by increasing steps of 10 °C. The sample electrode assembly (SEA) consisted of two stainless-steel electrodes (20 mm diameter) filled with the sample. The proton conductivity (σ_{Prot}) of the polyelectrolytes was calculated according to **Equation 2**.

$$\sigma_{Prot} = \frac{L}{A \cdot R_0} \qquad \textbf{(2)}$$

where L is the thickness of the polyelectrolytes in cm, A is the area of the electrode in contact with the membrane in cm^2, and R_0 is the protonic resistance in Ω. The value of R_0 was taken from the Bode plot in the high-frequency range, in which the value of $log\ |Z|$ tends to a non-frequency-dependent asymptotic value and the phase angle reaches its maximum value.

The electric conductivity (σ_{dc}) was also measured from **Equation 2** with the values of R_0 at low frequencies, where the measured real part of the conductivity reaches a plateau. This method was explained in detail when exposed and described the results.

3. Results and discussion

The hydrothermal stability was preliminarily evaluated as a technological validation assay. Next, the physicochemical properties of the photo-crosslinked and post-sulfonated membranes were assessed in terms of structural characterization, thermal properties, and thermo-oxidative stability. Finally, the best candidates were validated in fuel cell experiments and the electrical and protonic conductivity were deeply characterized and correlated to fuel cell behavior.

3.1. Hydrothermal stability

The study of the mass variation as a function of time when immersed in water at 60 °C was considered as a preliminary method to simulate the service conditions and ascertain the membrane hydrothermal stability during 500 min. As displayed in **Figure 2**, the successive preparation steps of crosslinking and sulfonation were evaluated. The prepared membranes showed different behavior, which can be separated into three tendencies.

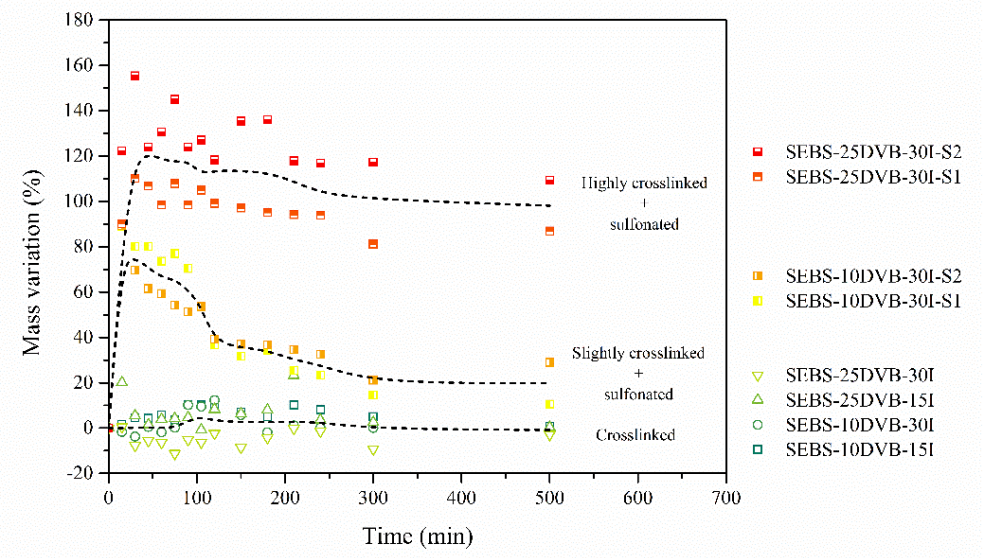

Figure 2. Mass variation as a function of immersion time for the photo-crosslinked and post-sulfonated SEBS-based membranes. Standard deviation between 2 and 10% was omitted for the sake of clarity.

The mass of the SEBS-10DVB and SEBS-25DVB crosslinked membranes was almost constant and the specimens remained unaltered during immersion regardless of the photo-irradiation time. In these compositions, mass variation remained in the ±5% range during immersion until the end of the assay. Although they were hydrolytically stable for the evaluated period, the absorbed humidity is still below the desired uptake for enhancing the vehicular mechanism for proton transport. The presence of a highly reticulated network in these membranes prevented the water penetration and reduced their swelling capability.

Even though the photo-crosslinking endorsed hydrothermal stability to the membranes, the incorporation of sulfonic groups may alter their hydrophilicity and thereby their hydrothermal stability. To understand the consequences of the sulfonation, the membranes with the higher photo-irradiation time (30 min) and both sulfonation conditions (S1 and S2) were assessed.

For a 10%wt. DVB in the SEBS-10DVB-30I-S1, SEBS-10DVB-30I-S2 membranes, the mass increased in the first stage of immersion reaching near 70%, and then decreased to percentages between 20 and 30%. Given that water desorption may not be understood at equilibrium, the release of polymer segments from the membrane may be the cause of the perceived mass loss. As well, although mass was measurable until the end of the assay, these membranes were fragmented during the swelling analyses.

When the DVB content increased up to 25%wt. in the SEBS-25DVB-30I-S1 and SEBS-25DVB-30I-S2 membranes, the mass variation increased up to percentages between 100 and 150% but it remained stable until the end of the assay, indicating that photo-crosslinking process with 25%wt. DVB was more effective in terms of hydrothermal stability. The higher contribution of the DVB in these compositions retained the mechanical integrity during swelling, essential for PEM applications. Moreover, the membranes with the strongest post-sulfonation conditions resulted in slightly higher water absorption capability due to the higher presence of sulfonic groups that enhanced the hydrophilicity of these membranes.

In general, it was recognized that the membranes with compositions involving higher DVB percentage permitted to achieve enough cross-linking to bring suitable hydrolytic stability, and the post-sulfonation reaction enhanced the water uptake ability of the membranes. From this point onwards, the characterization and validation analyses were therefore focused on the crosslinked membranes with 25%wt. DVB and post-sulfonated. The non-crosslinked blends and the non-sulfonated membranes were included in further sections for comparison purposes.

3.2. Membrane characterization

3.2.1. Chemical structure

The structural characterization through Fourier transformed infrared spectroscopy (FT-IR) allows for the identification of the functional groups and composition of the different membranes. The spectra collected in the range of 4000-500 cm^{-1} of the uncrosslinked, photo-crosslinked, and post-sulfonated SEBS-25DVB-based compositions are plotted in **Figure 3**.

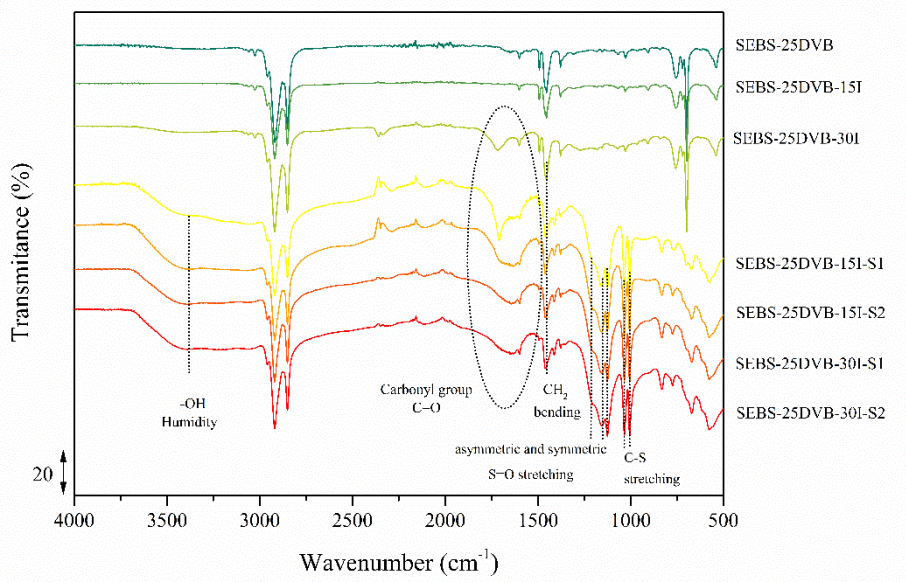

Figure 3. FT-IR spectra of the uncrosslinked, photo-crosslinked, and post-sulfonated SEBS-25DVB-based membranes.

In general, the structure of the polystyrene segments was corroborated by the peak observed at 3025 cm^{-1}, which corresponds to C-H aromatic stretching, and those at 2917 cm^{-1} and 2850 cm^{-1} referred to as C-H aliphatic stretching. The absorption at 1600 cm^{-1} is attributed to the phenyl ring of polystyrene and strong vibrations at 1490 and 1450 cm^{-1} are assigned to the stretching of C=C aromatic bonds [29]. The strong absorption bands at 759 and 538 cm^{-1} are attributed to C-H out-of-plane bending [32]. The characteristic peaks attributed to DVB could be found at 904 and 989 cm^{-1}, which are also typical bands of polystyrene (C-H in-plane bending) [29,32]. Given the similar structure of SEBS and DVB, peak overlapping may have occurred. Nevertheless, a slight absorption band around 1720 cm^{-1} could be appreciated, associated with carbonyl groups (C=O). The presence of these carbonyl groups in the membrane could be ascribed to the oxidation of DVB molecules during dissolution and solvent evaporation. Therefore, this peak may indirectly confirm the presence of DVB in the membranes.

When irradiated, two complementary very intense peaks were observed at 1720 cm^{-1} and 1270 cm^{-1}. The vibration of the carbonyl group (C=O) and the C-O stretching could be identified, respectively. Moreover, a broadband at 3400 cm^{-1} due to the stretching of hydroxyl groups (O-H) was found [33]. In this regard, the photoirradiation process carried out in the presence of oxygen may have promoted secondary photo-oxidation reactions of the non-reacted DVB molecules and the feasible generation of carboxyl and hydroxyl groups [34].

The sulfonation reaction was corroborated by the presence of the signals in the range from 900 to 1400 cm^{-1}. Particularly, the bands at 1160 and 1215 cm^{-1} are due to the symmetric and asymmetric stretching vibration of the S=O group. The presence of $-SO_3^-$ could be also identified using the peak at 1030 and 1004 cm^{-1}, attributed to the in-plane bending of the para-substituted phenyl ring. Complementarily, a very intense peak associated with vibration of C-S bonds was detected at 1124 cm^{-1}. Moreover, a broadband was found in the sulfonated membranes between 3300 and 3600 cm^{-1} related to the hydroxyl group stretching (-OH) and justified by the presence of sulfonic groups that may have increased the hydrophilicity of the material. The post-sulfonation reaction may have affected the aromatic ring of polystyrene. The intensity of the peaks associated with the vibration of polystyrene phenolic ring at 1600 cm^{-1} and the stretching of the $-CH_2-$ bonds at 1450 cm^{-1} became less intense with increasing the sulfonation. Although no major differences were found, the diverse degree of sulfonation was noted by the intensity of the band associated with the sulfonic groups. The band strength slightly increased for the membranes with the strongest sulfonation conditions and was more visible in the SEBS-25DVB-30I-S2 membrane, involving the highest crosslinked structure and most severe sulfonation reaction. According to previous work with SEBS-based membranes [29], the proposed structure for the photo-crosslinked and post-sulfonated membranes is shown in **Figure 4**.

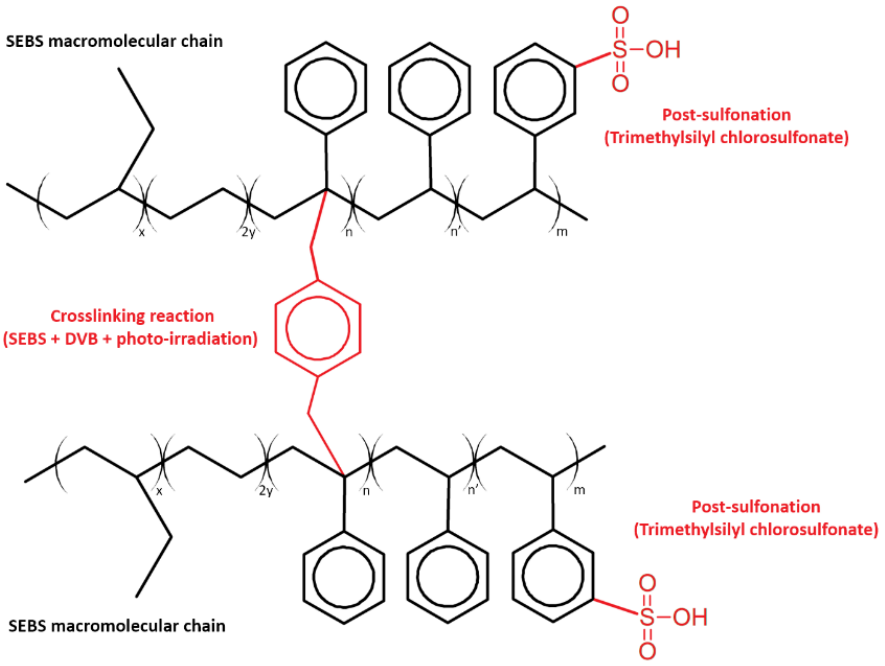

Figure 4. Scheme of the proposed structure for the photo-crosslinked and post-sulfonated membranes.

3.2.2. Thermal properties

The thermal properties of the membranes were characterized by differential scanning calorimetry (DSC). For this purpose, a controlled program under an inert atmosphere was carried out. The obtained thermograms of the first heating scan of the uncrosslinked, photo-crosslinked, and post-sulfonated SEBS-25DVB-based membranes are shown in **Figure 5**.

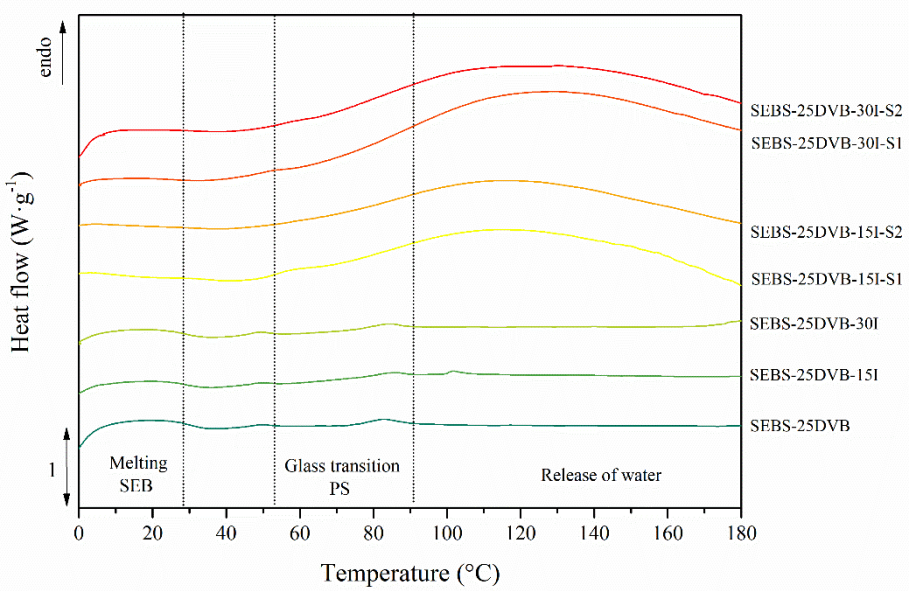

Figure 5. DSC thermograms of the uncrosslinked, photo-crosslinked, and post-sulfonated SEBS-25DVB-based membranes.

In the range from 0 to 30 °C, a strong endothermic peak was found attributed to the melting of the elastomer block of ethylene-butylene (EB). Then, a slight thermal event was perceived in the blend SEBS-25DVB and the crosslinked membranes between 70 and 90 °C due to the glass transition of PS segments [32]. Given the covalent bond formation between DVB and PS after photo-crosslinking and subsequent steric hindrance, the glass transition temperature (T_g) of PS increased from 82.8 up to 84.4 °C.

The thermograms of the sulfonated membranes showed a different trend. First, the endothermic peak due to the melting of the EB segment was slightly lower. Then, in the temperature range between 70 and 160 °C, a broad endothermic peak was observed, caused by the release of water and the disorder transition of the cluster phase. Given the broad peak, the release of both free water molecules superficially absorbed and bound water interacting with the sulfonic groups through hydrogen bonding were expected. The presence of such an intense endothermic peak may have overlapped the T_g of the PS segments, so the second heating scan served to evaluate it. However, a very small glass transition could be evaluated in the second heating scan. The T_g of the PS segments and the temperatures of the release of water (T_{water}) are gathered in Table 2.

Table 2. Glass transition (T_g) of PS segments and water release (T_{water}) temperatures of uncrosslinked, photo-crosslinked, and post-sulfonated membranes, as obtained from the second heating scan.

	$T_{g\ PS}$ (°C)	T_{water} (°C)
SEBS-25DVB	82.8±0.4	-
SEBS-25DVB-15I	84.0±1.3	-
SEBS-25DVB-30I	84.4±0.8	-
SEBS-25DVB-15I-S1	87.7±1.1	115.9±1.9
SEBS-25DVB-15I-S2	88.2±0.9	116.4±1.7
SEBS-25DVB-30I-S1	92.8±1.8	129.4±2.5
SEBS-25DVB-30I-S2	92.6±1.3	129.9±2.1

On the one hand, a slight increase in the T_g of PS was observed in the sulfonated membranes. Given the sulfonation reaction that attached the sulfonic groups to the aromatic rings and reduced the mobility of PS segments, the overall contribution to the glass transition diminished and it was displaced towards higher temperatures. On the other hand, the T_{water} was greater in the higher crosslinked membranes, regardless of the sulfonation reaction. The presence of a more compact structure with a more tortuous pathway for water release may have contributed to this increase. Although the presence of more sulfonic groups would result in higher hydrophilicity, non-significant differences in T_{water} were observed for the membranes with different sulfonation conditions.

3.2.3. Thermo-oxidative stability

The thermal stability and decomposition profiles of the membranes under oxidative atmosphere were assessed through thermogravimetric analysis (TGA). The weight loss as a function of time was studied during dynamic experiments and the thermogravimetric thermograms (TG) were obtained. Furthermore, the first-order derivative curve (DTG), which provides specific information about the different degradation stages and peak temperatures, was calculated. Both TG and DTG curves of the uncrosslinked, photo-crosslinked, and post-sulfonated SEBS-25DVB-based membranes are plotted in **Figure 6**. For a deeper evaluation, the onset of the degradation (T_{onset}) as the 5% of mass loss was calculated. Moreover, the peak temperature and mass loss of water release (T_{water}, ΔW_A) and decomposition stages (T_A, T_B, T_C, ΔW_A, ΔW_B, ΔW_C) were obtained and are gathered in **Table 3**.

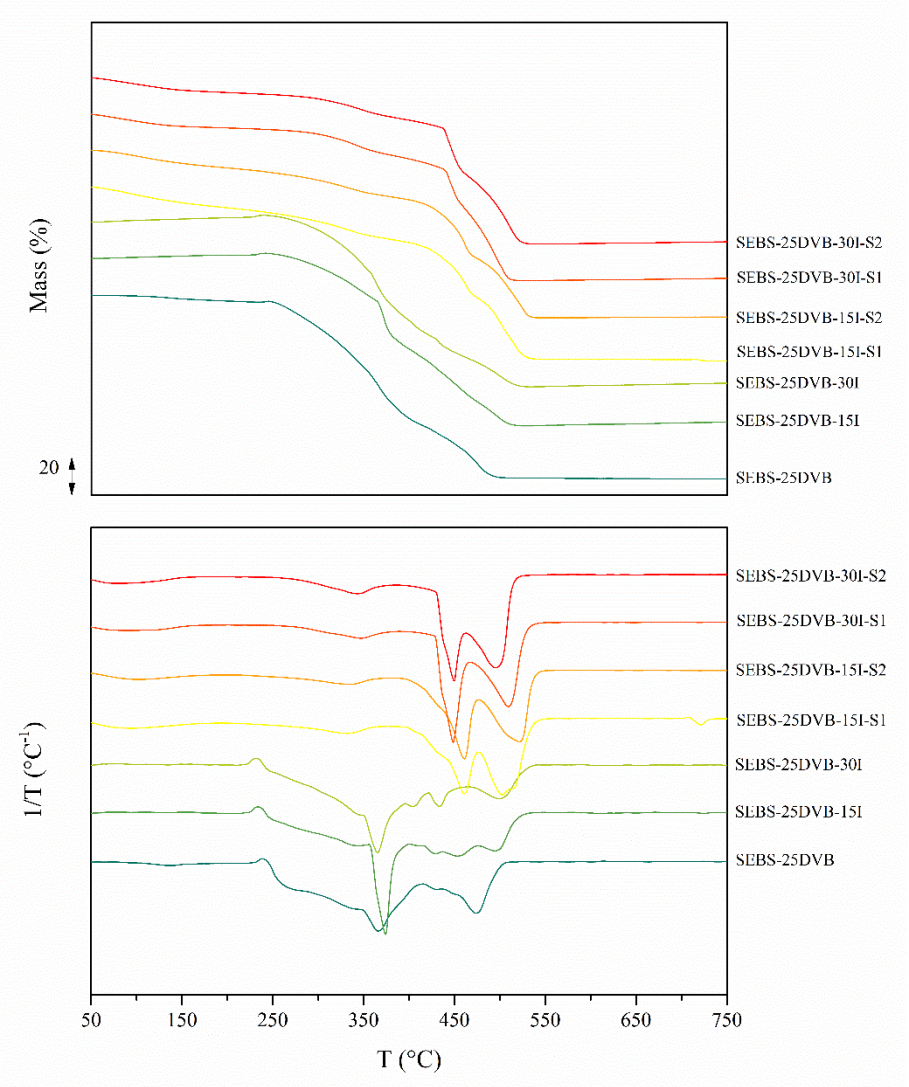

Figure 6. Thermogravimetric (up) and derivative thermogravimetric curves (DTG) (down) of the uncrosslinked, photo-crosslinked, and post-sulfonated SEBS-25DVB-based membranes.

In general, a multiple-stage mass loss behavior was found in all the compositions. In particular, two significant decomposition stages were observed in the SEBS-25DVB blend. The first stage from 240 to 420 °C involved the mass loss due to the decomposition of the aromatic rings of polystyrene and DVB molecules and the second stage from 420 to 550 °C was attributed to the polymeric backbone decomposition.

After photo-irradiation and subsequent crosslinking, similar thermo-oxidative decomposition profiles were found. However, the onset decomposition temperature (T_{onset}) was displaced towards higher temperatures. In general, the crosslinking process retarded the thermo-oxidative decomposition and therefore increased the stability of the membranes. Although 15 min of photoirradiation increased the onset from 256.8 °C up to 304.5 °C, the longest photoirradiation time of 30 min resulted in a slightly lower increase up to 301.7 °C. The high photo-oxidation of the DVB molecules during the crosslinking reaction and subsequent generation of oxidized functional groups may be responsible for this behavior. Indeed, the peak decomposition temperatures of both stages of the aromatic ring and polymer backbone decomposition (T_1 and T_2) increased after crosslinking for 15 min but decreased after 30 min of crosslinking. Particularly, the decrease in the temperature for the backbone decomposition was significant, moving from 489.4 °C for the uncrosslinked to 430.4 °C for the 30 min crosslinked membrane.

Table 3. Temperature peak and weight losses of the different thermo-oxidative decomposition stages of the uncrosslinked, photo-crosslinked, and post-sulfonated SEBS-25DVB-based membranes. Standard deviation between 1 and 2% was omitted for the sake of clarity.

	Water release		**Decomposition**						
	T_{water} (°C)	ΔW_{water} (%)	T_{onset} (°C)	**Stage A (Sulfonic and hydroxyl group)**		**Stage B (PS and DVB)**		**Stage C (Backbone)**	
				T_A (°C)	ΔW_A (%)	T_B (°C)	ΔW_B (%)	T_C (°C)	ΔW_C (%)
SEBS-25DVB	-	-	256.8	-	-	365.7	66.7	473.4	30.1
SEBS-25DVB-15I	-	-	304.5	-	-	374.2	55.3	498.5	35.7
SEBS-25DVB-30I	-	-	301.7	-	-	361.6	53.2	498.8	35.6
SEBS-25DVB-15I-S1	99.7	8.4	292.4	333.0	16.7	460.9	35.1	504.7	31.1
SEBS-25DVB-15I-S2	95.0	6.7	286.3	332.2	19.6	461.8	33.3	521.7	34.5
SEBS-25DVB-30I-S1	82.7	7.4	316.6	342.6	16.8	447.9	34.6	490.2	33.5
SEBS-25DVB-30I-S2	90.7	8.4	319.9	348.4	15.6	450.0	32.8	494.3	35.3

In the sulfonated membranes, the mass loss profiles revealed four significant stages, instead of the two found for the non-sulfonated membranes. A slightly lower onset temperature was found in membranes sulfonated after 15 min of crosslinking, while sulfonation in those crosslinked during 30 min increased the onset. This behavior could be correlated to the crosslinking degree, which increased as a function of the photoirradiation time. It is important to remark that in

these membranes, given the humidity evaporation process, the onset was calculated as the 5% mass loss once mass was stabilized after water release.

The humidity evaporation stage with a percentage of around 10% occurred at temperatures below 100 °C and was due to the loss of free water. The presence of sulfonic groups in the membrane structure attracted and retained water molecules that were released during heating. Then, the next mass loss stage was found in the range from 250 to 360 °C and may be attributed to the hydroxyl group (-OH) decomposition along with $-SO_3^-$ group removal reactions [35,36]. Then, the degradation of aromatic compounds both from the polymer backbone and the crosslinking agent occurred. Given the high presence of aromatic rings, a significant contribution to the mass loss was found around 35%. Moreover, a significant displacement of the peak temperature of the degradation of polystyrene towards higher values from 360 °C to 460 °C was noted in the sulfonated membranes. The feasible generation of unsaturation during previous thermo-oxidative decomposition reactions may lead to the formation of conjugated structures and, therefore, the initial thermal stability was improved [36]. Finally, the fourth stage related to the degradation of the polymer backbone occurred at temperatures around 500 °C. This stage was also displaced towards higher values for the sulfonated membranes.

In general, although the presence of sulfonic groups may propose lower thermo-oxidative stability, it prevailed the stabilizing effect of the crosslinking reaction, as the onset temperature increased, particularly for the 30 min irradiated membranes. Moreover, the main degradation stages moved towards higher temperatures in all cases. Overall, all the sulfonated membranes remained stable up to 285 °C, highly above the service life temperature of these membranes as electrolytes.

3.3. Membrane validation

3.3.1. Fuel cell performance

The potential use of the proposed photo-crosslinked and post-sulfonated membranes as PEMFC electrolytes was investigated through their electrochemical performance in H_2/O_2 single cells. The results were acquired at atmospheric pressure, at 60 °C and 70 °C in saturated humidity conditions, and the recorded power density curves are shown in **Figure 7**. Likewise, electrochemical data in terms of open-circuit voltage (*OCV*), maximum current density (i_{max}), and maximum power density (W_{max}) values were obtained, and are displayed in **Table 4**.

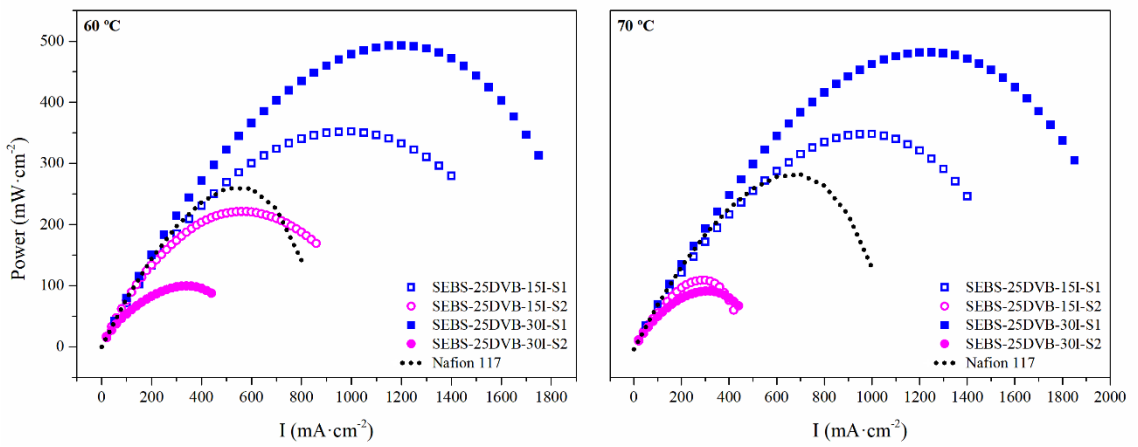

Figure 7. Power density curves at 60 °C (left) and 70 °C (right) of the photo-crosslinked and post-sulfonated SEBS-25DVB-based membranes.

Table 4. Electrochemical data of single-cell performance in terms of open-circuit voltage (*OCV*), maximum current density (i_{max}), and maximum power density (W_{max}) at 60 °C and 70 °C of the photo-crosslinked and post-sulfonated SEBS-25DVB-based membranes in comparison to Nafion 117®. The standard deviation between 1 and 4% was omitted for the sake of clarity.

	T_{cell} 60 °C			T_{cell} 70 °C		
	OCV **(V)**	i_{max} **(mA·cm^{-2})**	W_{max} **(mW·cm^{-2})**	***OCV*** **(V)**	i_{max} **(mA·cm^{-2})**	W_{max} **(mW·cm^{-2})**
Nafion 117®	1.016	800	259	0.998	1000	310
SEBS-25DVB-15I-S1	0.937	1400	352	0.934	1400	382
SEBS-25DVB-15I-S2	0.960	860	222	0.946	420	122
SEBS-25DVB-30I-S1	0.976	1750	493	0.977	1850	526
SEBS-25DVB-30I-S2	0.878	440	100	0.896	440	103

In general, higher temperatures improved the performance of the membranes. However, as can be observed and contrary to what initially seemed foreseeable, the membranes treated under milder sulfonation conditions, i.e. SEBS-25DVB-15I-S1 and SEBS-25DVB-30I-S1, performed much more satisfactorily than those subjected to a more intense sulfonation, which showed a considerably reduced cell performance. The obtained results suggest that an increase of the sulfonation extent may not necessarily imply a higher power density of the cell. Contrarily to the expectations, a remarkable decrease in power density was detected for the highest degree of sulfonation at both cell temperatures.

In terms of crosslinking, the best values were achieved for the membrane with 25%wt. DVB and the longest irradiation time. This behavior was perceivable at both cell temperatures. Indeed, if compared to commercially available membranes such as Nafion 117®, promising results were found. In particular, the SEBS-25DVB-30I-S1 almost doubled the acquired i_{max} and W_{max}. At this point, a deep understanding of electronic and ionic conductivities together

with analyzing their relationship with the molecular structure can give valuable information to comprehend and validate the results obtained in the fuel cell.

3.3.2. Electrical and protonic conductivity

Polymer electrolyte membrane fuel cells (PEMFC) require high electron selectivity to allow electrons to move through the external circuit together with a high proton conductivity to obtain high voltage per current density in the unit cell. Therefore, the evaluation of the electrical properties of the SEBS-25DVB photo-crosslinked and post-sulfonated membranes may offer knowledge on their conductivity mechanisms.

The electrical conductivity can be evaluated over a broad range of temperatures or frequencies [37]. In this study, the dependence on the frequency of the electrical conductivity was evaluated in the range from 10 °C to 90 °C, which results are plotted in **Figure 8**.

The electrical conductivity is composed of the alternating current (AC) and the direct current (DC) as shown in **Equation 3**.

$$\sigma_0(\omega) = \sigma_{dc} + \sigma_{ac} \qquad (3)$$

At high frequencies, the most important component of the conductivity is the AC (σ_{ac}), and the DC component (σ_{dc}) becomes almost negligible. It can be observed in **Figure 8** that the σ_{ac} values linearly decrease with the frequency and increase with the temperature, which indicates that electron conduction is thermally activated. Moreover, for specific temperatures, the plot presents a certain curvature that may indicate that the process is complex in which both dielectric relaxation and charge transport processes are contributing to conductivity. Particularly, the molecular movements that give rise to relaxations may be involved and subsequently alter the electrical conductivity [38].

In general, at low frequencies for a given temperature, it is expected a critical frequency at which the σ_{ac} shows a plateau and starts to be constant. Thus, the direct conductivity (σ_{dc}) can be estimated from this plateau. At this point, the DC component of the conductivity becomes independent of the frequency. **Figure 8** shows that the described conductivity plateaus are not visible in the analyzed membranes, and the conductivity continuously decreases as a function of frequency. This behavior can be understood due to the molecular structure of the assessed copolymers. In particular, the melting of ethylene-butylene block (from 0 to 30 °C) and the glass transition of the styrene block (~90 °C) determine the electric conductivity behavior. At low temperatures, only the ethylene-butylene molecular chains contribute to the electron

transport but, when the temperature increases, the styrene rings, and the attached sulfonic groups overcome the glass transition and also contribute to the conductivity [39].

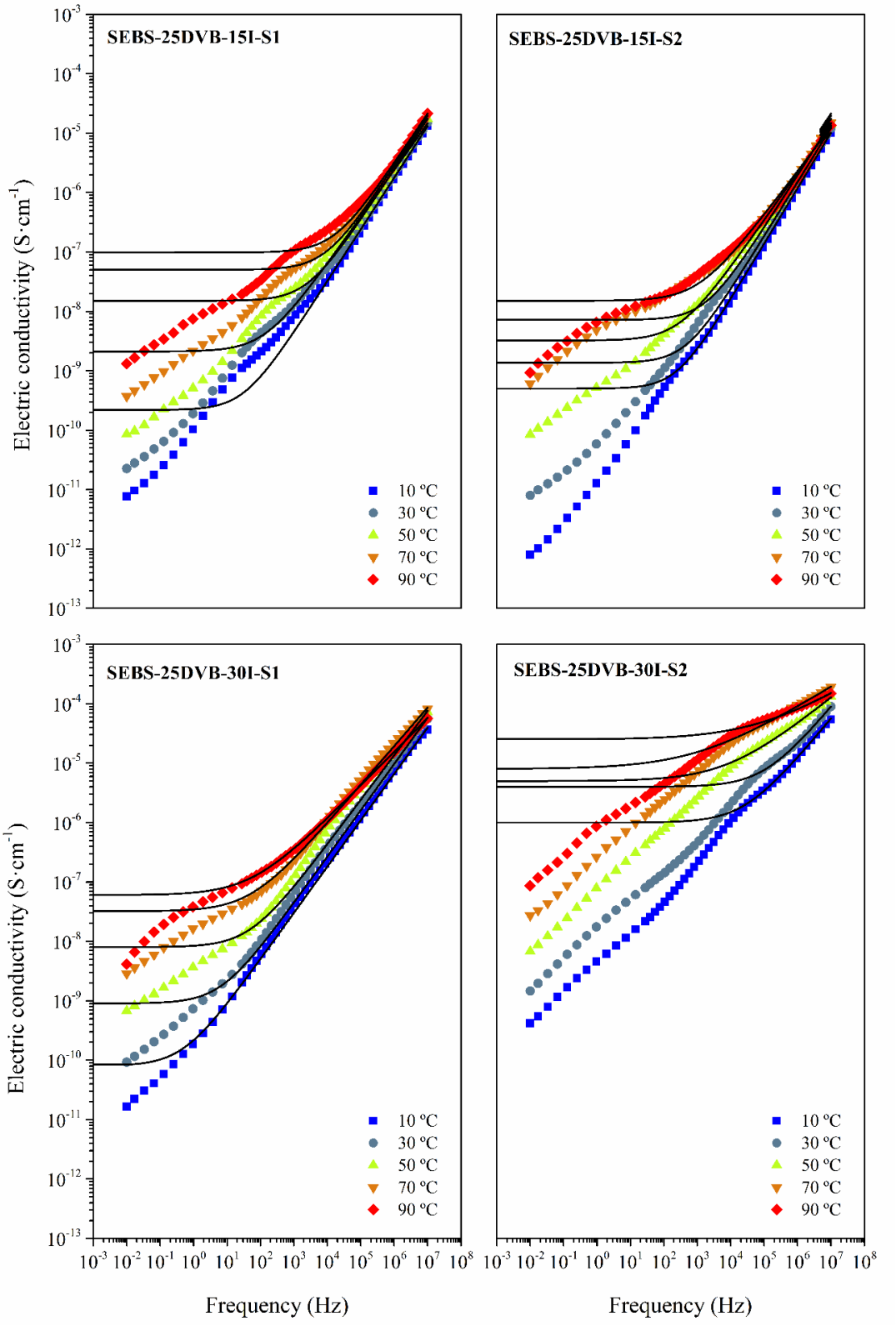

Figure 8. Isothermal curves (10 to 90 °°C) of the electrical conductivity as a function of frequency for the photo-crosslinked and sulfonated SEBS-25DVB-15I and SEBS-25DVB-30I membranes.

The temperature dependence of the electrical conductivity (σ_0) of the membranes was furtherly evaluated. The traditional method to obtain σ_0 takes into account the values of the direct electrical conductivity (σ_{dc}) calculated from the alternating current (σ_{ac}) curves, from the plateau in the low-frequency region [40–42]. However, considering the complexity of the obtained curves, the values were fitted to the universal power-law given by **Equation 4**.

$$\sigma(\omega) = \sigma_0 + A \cdot \omega^n \qquad (4)$$

where *A* is the pre-exponential factor and *n* is the fractional exponent varying from 0 to 1 [43,44]. The model curves of the power-law expression were included in **Figure 8** as solid lines, in which the plateau can be identified, where σ_{dc} is independent of the frequency. The conductivity could be therefore calculated at low frequencies, near to zero. The obtained values of the pre-exponential factor *A*, the fractional exponent *n*, and the conductivity (σ_0) are gathered in **Table 5**.

Table 5. Electrical conductivity (σ_0) of the photo-crosslinked and post-sulfonated SEBS-25DVB-based membranes in comparison to Nafion 117®. Standard deviation between 2 and 5% was omitted for the sake of clarity.

	T (°C)	$\sigma_0 \cdot 10^{10}$ (S·cm^{-1})	$A \cdot 10^{10}$	*n*	R^2
Nafion 117®	10	9000.00	2.75	0.07	0.986
	30	42500.00	66.75	0.01	0.997
	50	85300.00	17.00	0.01	0.999
	70	86800.00	144.00	0.02	0.994
	90	982000.00	995.00	0.02	0.985
SEBS-25DVB-15I-S1	10	2.18	0.02	0.87	0.999
	30	21.10	0.10	0.79	0.998
	50	150.00	0.04	0.85	0.999
	70	500.00	0.05	0.85	0.999
	90	978.00	0.06	0.84	0.999
SEBS-25DVB-15I-S2	10	5.00	0.01	0.93	0.999
	30	13.60	0.01	0.91	0.999
	50	32.20	0.08	0.80	0.996
	70	71.60	0.02	0.88	0.999
	90	150.00	0.21	0.74	0.989
SEBS-25DVB-30I-S1	10	0.80	0.33	0.78	0.992
	30	9.00	0.48	0.78	0.997
	50	80.00	1.08	0.75	0.993
	70	320.00	7.38	0.65	0.995
	90	600.00	21.40	0.57	0.999
SEBS-25DVB-30I-S2	10	10000.00	2.77	0.68	0.994
	30	40000.00	4.03	0.68	0.975
	50	50000.00	331.50	0.46	0.984
	70	81300.00	3470.00	0.35	0.983
	90	250000.00	2350.00	0.35	0.867

In general, the σ_0 increased with the temperature according to expectations. However, it was difficult to establish the relationship between the increment of the conductivity and the

crosslinking and sulfonation. Although the membrane with longer crosslinking time and stronger sulfonation conditions revealed the highest conductivity, it is important to highlight that all of them revealed low enough and suitable electrical conductivity for their usage as PEMs in fuel cells.

If the fractional exponent is analyzed, it can be stated that values of *n* maybe 1 for ideal long-range pathways and 0.5 for diffusion-limited hopping mechanism [45]. The values of *n* are closer to 1 for the membranes with the lowest crosslinking time, i.e. the SEBS-25DVB-15I-S1 and SEBS-25DVB-15I-S2. This behavior would be representative of long-range pathways for electrons conduction. Nevertheless, in the membranes with a higher percentage of crosslinking agent and longest photo-irradiation time such as SEBS-25DVB-30I-S1 the value of *n* lies between 0.78 and 0.55. Finally, for the SEBS-25DVB-30I-S2, the *n* achieved values lower than 0.5, which is characteristic of diffusion-limited hopping pattern, given that electrons may find a tortuous pathway for transportation [39].

The relationship between the conductivity (σ_0) and the temperature was thoroughly evaluated. The conductivity was plotted in an Arrhenius map, which is often used to understand the nature of the charge transport processes [46]. **Figure 9** displays the temperature dependence of the conductivity up to the glass transition temperature of the styrene block (~90 °C). Although it is possible to observe a certain curvature, it is not clear enough for being adjusted to a Vogel Fulcher Tammann (VFT)-like equation. Accordingly, **Table 6** gathers the apparent activation energy (E_a) as obtained through an approximation to a linear Arrhenius law.

The obtained results suggest that the nature of the charge transport process follows the long-range pathways or vehicular model, despite other authors propose that the conductivity process of similar membranes is associated either with the onset of the lateral motions or a jump-diffusion of a molecule to another neighbor. Although it is mentioned that the mobility of the charge follows a diffusion-limited hopping model, the perceived differences may be explained given their conductivity measurements at temperatures above the glass transition of the styrene block. Indeed, for higher temperatures, the hopping sites would necessarily be closer to each other and the Grotthuss model could be also promoted [47–49].

Table 6 shows that the decrease of apparent activation energy (E_a) is related to the degree of sulfonation. In this line, the E_a for the SEBS-25DVB-15I-S2 and SEBS-25DVB-30I-S2 membranes is lower than that of the SEBS-25DVB-15I-S1 and SEBS-25DVB-30I-S1 compositions. When the sulfonation is higher and the molecules are more interrelated due to

crosslinking, the apparent activation energy decreases, and the electronic conduction capacity increases. This result suggests that the vehicular mechanism is prominent in the less sulfonated membranes, which may be stimulated by the moving vehicle, as H_2O usually requires larger energy. On the other hand, when the sulfonation is higher, the apparent activation energy seems low enough to consider the conduction of charges within a network of hydrogen bonds as diffusion-limited hopping mechanism. Nevertheless, it is difficult to determine accurately the particular mode in which electrical charges are transferred at such low temperatures, which are in the fuel cell service range [50–53]. In comparison to Nafion 117®, which also showed a linear correlation to the Arrhenius law, lower E_a was found in both compositions with the highest degree of sulfonation. However, for the mild-sulfonated membranes higher E_a was observed if compared to Nafion 117®. These results, along with their lower electrical conductivity corroborates the promising behavior of the mild-sulfonated membranes.

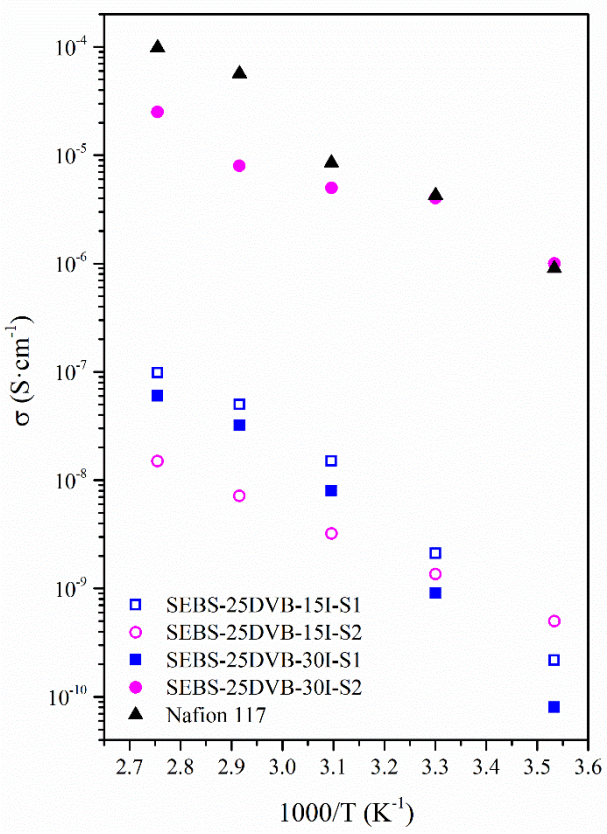

Figure 9. Arrhenius plot for the photo-crosslinked and post-sulfonated SEBS-25DVB-based membranes. Standard deviation between 2 and 5% was omitted for the sake of clarity.

Table 6. Activation energy (E_a) for the electrical conductivity of the photo-crosslinked and post-sulfonated SEBS-25DVB-based membranes.

	Slope	Intercept	E_a (kJ·mol^{-1})	R^2
Nafion 117®	-2.67	3.36	50.98	0.977
SEBS-25DVB-15I-S1	-3.80	3.46	72.72	0.971
SEBS-25DVB-15I-S2	-1.89	-2.63	36.19	0.999
SEBS-25DVB-30I-S1	-3.47	2.75	66.51	0.972
SEBS-25DVB-30I-S2	-1.59	-0.32	30.46	0.936

High proton conductivity is required to achieve an elevated maximum power in the unit cell [54]. Therefore, the proton conductivity (σ_{Prot}) of the photo-crosslinked and post-sulfonated membranes was evaluated to validate their performance as PEMs, through impedance spectroscopy. There are different methods to evaluate the relationship between the real and imaginary impedances on the frequency. The representation of the Bode plots was selected as a suitable method because it provides explicit information, while in the Nyquist and the Cole-Cole plots the impedance values remain hidden. **Figure 10** shows the Bode diagram, for the analyzed membranes in saturated humidity conditions. The calculated values of proton conductivity (σ_{Prot}) are shown in **Table 7** [54].

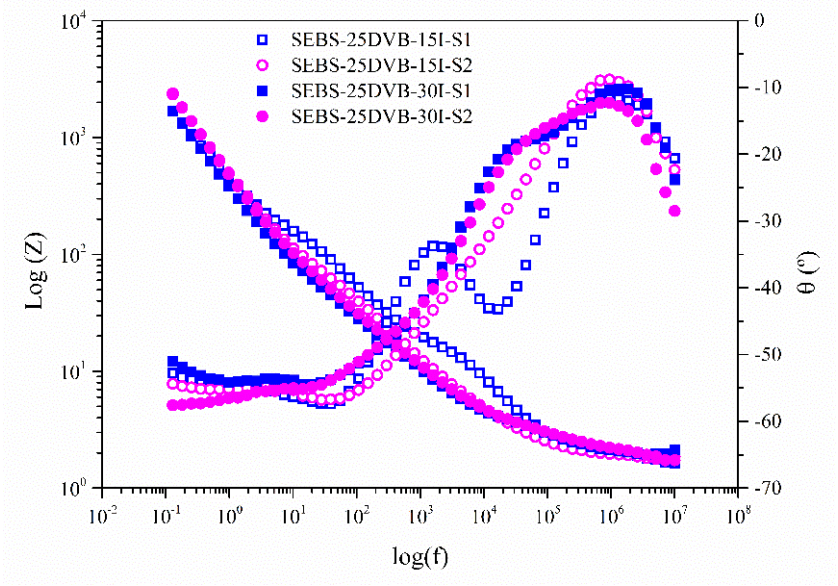

Figure 10. Bode diagrams and phase angle of the photo-crosslinked and post-sulfonated SEBS-25DVB-based membranes, measured at 70 °C.

Table 7. Proton conductivity (σ_{Prot}) of the photo-crosslinked and post-sulfonated SEBS-25DVB-based membranes in comparison to Nafion 117® at 70 °C.

	R_0 (Ω)	Thickness (mm)	σ_{Prot} (S·cm^{-1})
Nafion 117®	1.87	0.178	$3.0 \cdot 10^{-3}$
SEBS-25DVB-15I-S1	1.86	0.110	$1.9 \cdot 10^{-3}$
SEBS-25DVB-15I-S2	1.83	0.069	$1.2 \cdot 10^{-3}$
SEBS-25DVB-30I-S1	1.95	0.153	$2.5 \cdot 10^{-3}$
SEBS-25DVB-30I-S2	1.95	0.104	$1.7 \cdot 10^{-3}$

In line with fuel cell performance, the results indicate that membranes with a milder sulfonation such as SEBS-25DVB-15I-S1 and SEBS-25DVB-30I-S1 exhibit higher proton conductivities than those strongly sulfonated. Protons, coming from the acid groups confined within the polystyrene block domains, must be responsible for the ionic conductivity. Besides, **Figure 11** shows the correlation of the proton conductivity results with the maximum power density W_{max} obtained in the PEMFC performance tests. The SEBS-25DVB-30I-S1 membrane, with the highest crosslinking and the lowest sulfonation, was the more suitable composition, as it showed the best proton conduction capacity of $2.5 \cdot 10^{-3}$ S·cm^{-1}. Indeed, the obtained value was almost identical to that of the Nafion 117® membrane of $3.0 \cdot 10^{-3}$ S·cm^{-1}.

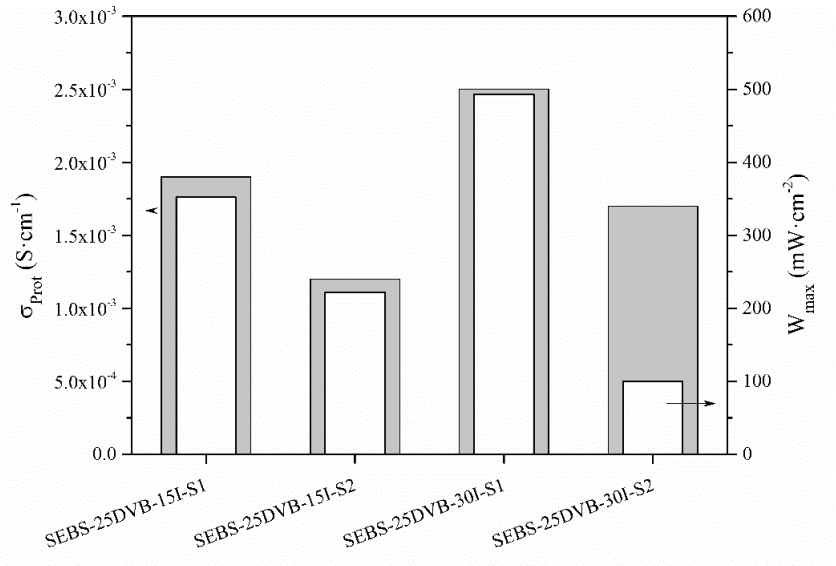

Figure 11. Comparison of proton conductivity (σ_{prot}) (grey bars) and maximum power density (W_{max}) (white bars), as measured through impedance and in fuel cell conditions of the crosslinked and sulfonated SEBS-25DVB-15I and SEBS-25DVB-30I membranes. Standard deviation between 2 and 10% was omitted for the sake of clarity.

As the above results suggest from the electrical conductivity model and apparent activation energy, both transport charge mechanisms could take place together in the SEBS-25DVB-30I-S1 membrane: the vehicular pattern with the aid of the diffusion of H_2O molecules and also

proton hopping along the chains of a hydrogen-bonded structure. However, in the SEBS-25DVB-30I-S2 membrane, due to the higher sulfonic group concentration, the proton hopping may prevail, while the vehicle mechanism may be impaired, which is a priority at the temperature operation of PEMFCs.

4. Conclusions

The evaluation of the physicochemical properties of the membranes allowed us to determine the optimal membrane preparation procedure for being used as electrolytes for proton exchange membranes in fuel cell applications.

Photo-crosslinked membranes of styrene-ethylene-butylene-styrene triblock copolymer (SEBS) with 25%wt. crosslinking agent divinyl-benzene (DVB) revealed superior hydrolytic stability than those with a lower percentage of DVB. The combination of SEBS with 25%wt. DVB and post-sulfonation allowed for water absorption as a function of time, reaching equilibrium with complete physical integrity. Although hydrophilicity of the membranes may have increased due to the post-sulfonation and the generation of carboxyl and hydroxyl groups due to the photo-oxidation of DVB molecules, it was not critical for compromising hydrolytic stability.

Due to the complexity of the conductivity curves, a universal power law was applied to obtain the electrical conductivity, which increased with temperature and crosslinking. The apparent activation energy relationship with temperature was approximated to a linear Arrhenius law. The nature of the charge transport process follows a long-range pathway or vehicular model in the studied temperature range. The obtained low electrical conductivity allowed these membranes for being used as electrolytes in proton exchange membrane fuel cells.

In terms of proton conductivity, promising results were found for membranes with the milder sulfonation treatment. In this line, the power density decreased for the higher degree of sulfonation. Overall, an increase of the sulfonation may not be strictly correlated to a better fuel cell behavior. Among all the compositions, the SEBS-25DVB-30I-S1 membrane with the highest crosslinking and the softer post-sulfonation conditions revealed a promising performance for being implemented as a cost-effective alternative electrolyte in hydrogen fuel cells.

Acknowledgments

The authors would like to thank the support of the European Union is through the European Regional Development Funds (ERDF) and the Spanish Ministry of Economy, Industry, and

Competitiveness, for the research projects ENE2017-86711-C3-1-R, ENE2017-90932-REDT. Universitat Politècnica de València is thanked for the PAID-10-19 SUB-1 grant for R. Teruel. Finally, Generalitat Valenciana is thanked for the APOSTD/2020/155 grant for O. Gil-Castell.

Data availability

The data that support the findings of this study are available from the corresponding author upon reasonable request.

Conflict of interest

The authors declare no conflicts of interest.

References

1. Ralph, T. R. *Platin. Met. Rev.* **2006**, *50*, 200.
2. Ma, J.; Sahai, Y. *Carbohydr. Polym.* **2013**, *92*, 955.
3. Ogungbemi, E.; Ijaodola, O.; Khatib, F. N.; Wilberforce, T.; El Hassan, Z.; Thompson, J.; Ramadan, M.; Olabi, A. G. *Energy* **2019**, *172*, 155.
4. Hasegawa, S.; Hiroki, A.; Ohta, Y.; Iimura, N.; Fukaya, A.; Maekawa, Y. *Radiat. Phys. Chem.* **2020**, *171*, 108647.
5. Zhang, C.; Yue, X.; Yang, Y.; Lu, N.; Zhang, S.; Wang, G. *J. Power Sources* **2020**, *450*, 227664.
6. Rozière, J.; Jones, D. J. *Annu. Rev. Mater. Res.* **2003**, *33*, 503.
7. Oroujzadeh, M.; Mehdipour-Ataei, S.; Esfandeh, M. *Eur. Polym. J.* **2013**, *49*, 1673.
8. Gil-Castell, O.; Galindo-Alfaro, D.; Sánchez-Ballester, S.; Teruel-Juanes, R.; Badia, J. D.; Ribes-Greus, A. *Nanomaterials* **2019**, *9*, 397.
9. Gil-Castell, O.; Teruel-Juanes, R.; Arenga, F.; Salaberria, A. M.; Baschetti, M. G.; Labidi, J.; Badia, J. D.; Ribes-Greus, A. *React. Funct. Polym.* **2019**, *142*, 213.
10. Martínez-Felipe, A.; Moliner-Estopiñán, C.; Imrie, C. T.; Ribes-Greus, A. *J. Appl. Polym. Sci.* **2012**, *124*, 1000.
11. González-Guisasola, C.; Ribes-Greus, A. *Polym. Test.* **2018**, *67*, 55.
12. Gil-Castell, O.; Cerveró, R.; Teruel-Juanes, R.; Badia, J. D. D.; Ribes-Greus, A. *J. Renew. Mater.* **2019**, *7*, 655.
13. Hu, M.; Zhang, B.; Chen, J.; Xu, M.; Liu, D.; Wang, L. *Int. J. Energy Res.* **2019**, *43*, er. 4879.
14. Liaqat, K.; Rehman, W.; Saeed, S.; Waseem, M.; Fazil, S.; Shakeel, M.; Kang, P. *Solid State Ionics* **2018**, *319*, 141.
15. Miyatake, K.; Furuya, H.; Tanaka, M.; Watanabe, M. *J. Power Sources* **2012**, *204*, 74.
16. Yao, H.; Shi, K.; Song, N.; Zhang, N.; Huo, P.; Zhu, S.; Zhang, Y.; Guan, S. *Polymer (Guildf).* **2016**, *103*, 171.
17. Pan, H.; Chen, S.; Jin, M.; Chang, Z.; Pu, H. *Ionics (Kiel).* **2018**, *24*, 1629.
18. Nambi Krishnan, N.; Konovalova, A.; Aili, D.; Li, Q.; Park, H. S.; Jang, J. H.; Kim, H.-J.; Henkensmeier, D. *J. Memb. Sci.* **2019**, *588*, 117218.
19. Asensio, J. A.; Sánchez, E. M.; Gómez-Romero, P. Proton-conducting membranes based on benzimidazole polymers for high-temperature PEM fuel cells. A chemical quest. *Chem. Soc. Rev.* **2010**, *39*, 3210–3239.
20. Krishnan, N. N.; Lee, H. J.; Kim, H. J.; Kim, J. Y.; Hwang, I.; Jang, J. H.; Cho, E. A.; Kim, S. K.;

Henkensmeier, D.; Hong, S. A.; Lim, T. H. *Eur. Polym. J.* **2010**, *46*, 1633.

21. Hickner, M. A.; Ghassemi, H.; Kim, Y. S.; Einsla, B. R.; McGrath, J. E. *Chem. Rev.* **2004**, *104*.
22. Gao, S.; Xu, H.; Luo, T.; Guo, Y.; Li, Z.; Ouadah, A.; Zhang, Y.; Zhang, Z.; Zhu, C. *J. Memb. Sci.* **2017**, *536*, 1.
23. Fu, F.; Xu, H.; Dong, Y.; He, M.; Zhang, Z.; Luo, T.; Zhang, Y.; Hao, X.; Zhu, C. *J. Memb. Sci.* **2015**, *489*, 119.
24. Date, B.; Han, J.; Park, S.; Park, E. J.; Shin, D.; Ryu, C. Y.; Bae, C. *Macromolecules* **2018**, *51*, 1020.
25. Fernández-Carretero, F. J.; Compañ, V.; Riande, E. *J. Power Sources* **2007**, *173*, 68.
26. Sangeetha, D. *Eur. Polym. J.* **2005**, *41*, 2644.
27. Jetsrisuparb, K.; Balog, S.; Bas, C.; Perrin, L.; Wokaun, A.; Gubler, L. *Eur. Polym. J.* **2014**, *53*, 75.
28. Navarro, A.; del Río, C.; Acosta, J. L. *J. Memb. Sci.* **2007**, *300*, 79.
29. del Río, C.; García, O.; Morales, E.; Escribano, P. G. *Electrochim. Acta* **2015**, *176*, 378.
30. Zawodzinski, T. A. *J. Electrochem. Soc.* **1993**, *140*, 1041.
31. Neogi, P. *Diffusion in Polymers*; Marcel Dekker, **1996**; Vol. 32.
32. Müller, F.; Ferreira, C. A.; Franco, L.; Puiggalí, J.; Alemán, C.; Armelin, E. *J. Phys. Chem. B* **2012**, *116*, 11767.
33. Chen, S. L.; Benziger, J. B.; Bocarsly, A. B.; Zhang, T. *Ind. Eng. Chem. Res.* **2005**, *44*, 7701.
34. Luengo, C.; Allen, N. S.; Edge, M.; Wilkinson, A.; Parellada, M. D.; Barrio, J. A.; Santa, V. R. *Polym. Degrad. Stab.* **2006**, *91*, 947.
35. Kerres, J. A.; Katzfuß, A.; Chromik, A.; Atanasov, V. *J. Appl. Polym. Sci.* **2014**, *131*, n/a.
36. Zhu, X.; Elomaa, M.; Sundholm, F.; Lochmüller, C. H. *Polym. Degrad. Stab.* **1998**, *62*, 487.
37. Salam, F.; Soulayman, S. S.; Giuntini, J. C.; Zanchetta, J. V *Solid state ionics* **1996**, *83*, 235.
38. Chan, C. H.; Kammer, H.-W. *Ionics (Kiel).* **2017**, *23*, 2327.
39. Hunt, A. *J. Non. Cryst. Solids* **1993**, *160*, 183.
40. Elliott, S. R. *Adv. Phys.* **1987**, *36*, 135.
41. Elliott, S. R. *Philos. Mag.* **1977**, *36*, 1291.
42. Pollak, M.; Geballe, T. H. *Phys. Rev.* **1961**, *122*, 1742.
43. Jonscher, A. K. *Nature* **1977**, *267*, 673.
44. Jonscher, A. K. *J. Phys. D. Appl. Phys.* **1999**, *32*, R57.
45. Mauritz, K. A. *Macromolecules* **1989**, *22*, 4483.
46. Pradhan, D. K.; Choudhary, R. N. P.; Samantaray, B. K. *Int. J. Electrochem. Sci.* **2008**, *3*, 597.
47. Stickel, F.; Fischer, E. W.; Richert, R. *J. Chem. Phys.* **1995**, *102*, 6251.
48. Wojnarowska, Z.; Wang, Y.; Pionteck, J.; Grzybowska, K.; Sokolov, A. P.; Paluch, M. *Phys. Rev. Lett.* **2013**, *111*, 225703.
49. Chen, H.; Hassan, M. K.; Peddini, S. K.; Mauritz, K. A. *Eur. Polym. J.* **2011**, *47*, 1936.
50. Kreuer, K.-D. *Chem. Mater.* **1996**, *8*, 610.
51. Kreuer, K.-D.; Rabenau, A.; Weppner, W. *Angew. Chemie Int. Ed. English* **1982**, *21*, 208.
52. Ramaswamy, P.; Wong, N. E.; Shimizu, G. K. H. *Chem. Soc. Rev.* **2014**, *43*, 5913.
53. Agmon, N. *Chem. Phys. Lett.* **1995**, *244*, 456.
54. Lee, C. H.; Park, H. B.; Lee, Y. M.; Lee, R. D. *Ind. Eng. Chem. Res.* **2005**, *44*, 7617.

Graphical abstract

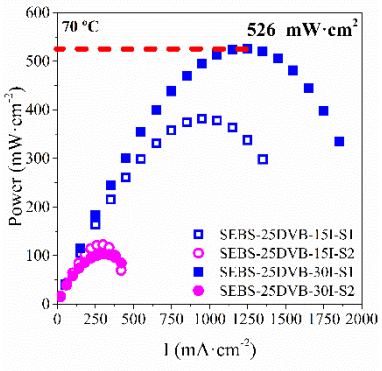

ANNEX. OPEN ACCESS POLICIES

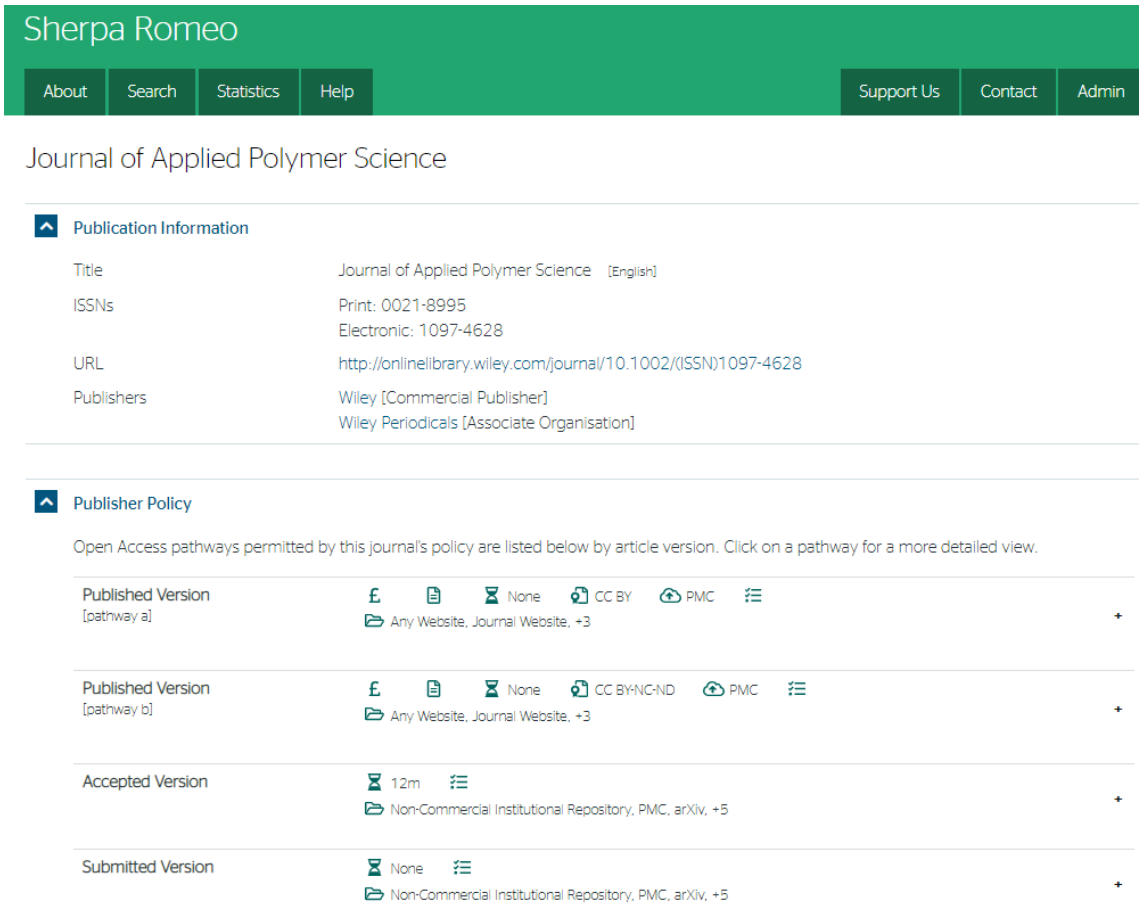

Sherpa Romeo

About | Search | Statistics | Help | Support Us | Contact | Admin

Journal of Applied Polymer Science

Publication Information

Title	Journal of Applied Polymer Science [English]
ISSNs	Print: 0021-8995 Electronic: 1097-4628
URL	http://onlinelibrary.wiley.com/journal/10.1002/(ISSN)1097-4628
Publishers	Wiley [Commercial Publisher] Wiley Periodicals [Associate Organisation]

Publisher Policy

Open Access pathways permitted by this journal's policy are listed below by article version. Click on a pathway for a more detailed view.

Published Version [pathway a]	£ None CC BY PMC Any Website, Journal Website, +3	+
Published Version [pathway b]	£ None CC BY-NC-ND PMC Any Website, Journal Website, +3	+
Accepted Version	12m Non-Commercial Institutional Repository, PMC, arXiv, +5	+
Submitted Version	None Non-Commercial Institutional Repository, PMC, arXiv, +5	+